



Titre: Secondary ice production improves simulations of freezing rain
Title:

Auteurs: Méliissa Cholette, Jason A. Milbrandt, Hugh Morrison, Sabrina Kirk, &
Authors: Louis-Émile Lalonde

Date: 2024

Type: Article de revue / Article

Référence: Cholette, M., Milbrandt, J. A., Morrison, H., Kirk, S., & Lalonde, L.-É. (2024).
Citation: Secondary ice production improves simulations of freezing rain. Geophysical
research letters, 51(8), 108490 (11 pages). <https://doi.org/10.1029/2024gl108490>

 **Document en libre accès dans PolyPublie**
Open Access document in PolyPublie

URL de PolyPublie: <https://publications.polymtl.ca/58183/>
PolyPublie URL:

Version: Version officielle de l'éditeur / Published version
Révisé par les pairs / Refereed

Conditions d'utilisation: CC BY-NC-ND
Terms of Use:

 **Document publié chez l'éditeur officiel**
Document issued by the official publisher

Titre de la revue: Geophysical research letters (vol. 51, no. 8)
Journal Title:

Maison d'édition: Wiley
Publisher:

URL officiel: <https://doi.org/10.1029/2024gl108490>
Official URL:

Mention légale: © 2024 His Majesty the King in Right of Canada and The Authors. Reproduced with the
Legal notice: permission of the Minister of Environment and Climate Change Canada. This is an open
access article under the terms of the Creative Commons Attribution-NonCommercial-
NoDerivsLicense, which permits use and distribution in any medium, provided the
original work is properly cited, the use is non-commercial and no modifications or
adaptations are made.

Geophysical Research Letters®



RESEARCH LETTER

10.1029/2024GL108490

Key Points:

- Secondary ice production (SIP) substantially impacts precipitation phase and type in winter storms
- Inclusion of SIP reduces excessive freezing rain (FR) in numerical simulations
- Forecast metrics for FR in 40 winter cases are improved when SIP is included in a weather model

Supporting Information:

Supporting Information may be found in the online version of this article.

Correspondence to:




M. Cholette,
melissa.cholette@ec.gc.ca

Citation:

Cholette, M., Milbrandt, J. A., Morrison, H., Kirk, S., & Lalonde, L.-É. (2024). Secondary ice production improves simulations of freezing rain. *Geophysical Research Letters*, 51, e2024GL108490. <https://doi.org/10.1029/2024GL108490>

Received 17 OCT 2023
Accepted 3 APR 2024

Secondary Ice Production Improves Simulations of Freezing Rain

Mélissa Cholette¹ , Jason A. Milbrandt¹, Hugh Morrison² , Sabrina Kirk³ , and Louis-Émile Lalonde⁴

¹Meteorological Research Division, Environment and Climate Change Canada, Dorval, QC, Canada, ²National Center for Atmospheric Research, Boulder, CO, USA, ³Polytechnique Montréal, Montreal, QC, Canada, ⁴University of Montreal, Montreal, QC, Canada

Abstract Weather forecasts and climate projections of precipitation phase and type in winter storms are challenging due to the complicated underlying microphysical and dynamical processes. In the Canadian numerical weather prediction model, explicit freezing rain (FR) at the surface is often overestimated during the winter season for situations in which snow is observed. For a case study simulated using this model with the Predicted Particle Properties (P3) microphysics scheme, the secondary ice production (SIP) process has a major impact on the surface precipitation type. Parameterized SIP substantially reduces FR due to increased collection of supercooled drops with ice particles formed by rime splintering. Hindcast simulations of 40 winter cases show that these results are systematic, and the decreased frequency of FR leads to improved forecast skill relative to observations. Thus, accounting for SIP in the model is critical for accurately simulating precipitation types.

Plain Language Summary Several types of winter precipitation, including snow, freezing rain (FR) and ice pellets (IP), are associated with hazards such as injuries from people falling, disruption of electrical supply, and breakdown of transportation networks due to the accumulation of ice on surfaces. Forecasts of precipitation type using weather prediction models, as well as projections for a warmer climate, are challenging because of the complicated physical processes involved. In this article, it is shown that the component of the numerical model that is used to represent clouds and precipitation in the Canadian high-resolution weather forecast system overestimates FR at the expense of snow. This problem is mitigated when the additional process of secondary ice production (here, the generation of new ice particles from collisions of existing ice and supercooled drops) is included in the model. The presence of numerous small ice particles formed by this process decreases the amount of FR and improves forecast skill scores for 40 historic winter cases. Thus, accounting for this process in weather and climate models is important for accurately simulating FR, IP and snow.

1. Introduction

Several precipitation types can occur during winter storms in Canada and elsewhere, including snow, wet snow, ice pellets (IP), FR, and rain (e.g., Stewart et al., 2015). Ice pellets and especially FR are frequent over eastern Canada (e.g., Bresson et al., 2017; Cortinas et al., 2004; McCray et al., 2019). Freezing rain is associated with several hazards resulting from the accumulation of ice on surfaces, including injuries from people falling, disruption to the electrical grid, and breakdown of air and ground transportation (e.g., Chang et al., 2007; King & Laplante, 2005; Lecompte et al., 1998). The frequency, intensity and phase of winter precipitation types are expected to change in a warmer climate. However, the sign of the change (i.e., increase or decrease) will likely vary across regions and seasons. For example, over eastern Canada, there is no consensus on whether FR will increase or decrease in a warmer climate (e.g., Cheng et al., 2007, 2011; Lambert & Hansen, 2011; Matte et al., 2018).

The spatial distribution and timing of FR are challenging to predict, not only in climate models, but also in numerical weather prediction (NWP) models. Even a 1°C error in temperature can lead to an incorrect forecast of precipitation type, with rain instead of snow or FR instead of IP (e.g., Frick et al., 2013; Thériault et al., 2010). Apart from uncertainty associated with temperature predictions, many of the physical processes driving the evolution of these precipitation types remain uncertain (e.g., Ralph et al., 2005; Reeves et al., 2014). Hence, it is difficult to accurately simulate winter precipitation types in models (e.g., Barszcz et al., 2018).

Many weather forecasting centers use implicit (diagnostic) methods to predict the precipitation phase and type at the surface based on forecasted temperature and/or humidity profiles (e.g., Bourgouin, 2000; Elmore et al., 2015; Manikin et al., 2004). However, bulk microphysics schemes are used in almost all current weather (and climate) models, and they can provide detailed information on the phase and amount of surface precipitation based on the model-predicted precipitation variables. In these schemes, surface precipitation type is based on physical properties of the hydrometeors rather than being diagnosed from temperature and/or humidity (Cholette et al., 2020; Reeves et al., 2016; Thompson, 2019; Xu et al., 2019), thus representing a conceptual improvement over diagnostic methods. Environment and Climate Change Canada's High Resolution (2.5-km horizontal grid spacing) Deterministic Prediction System (HRDPS; Caron et al., 2021; Milbrandt et al., 2016) uses the Predicted Particle Properties (P3) bulk microphysics scheme (Milbrandt & Morrison, 2016; Morrison & Milbrandt, 2015). P3 uses a property-based approach to represent the continuum of ice-phase hydrometeor types. This contrasts with traditional schemes (e.g., Morrison et al., 2005; Seifert & Beheng, 2006; Thompson et al., 2004) that use pre-defined categories corresponding to specific types of ice particles (e.g., ice crystals, snow/aggregates, graupel). A recent development of P3 was the prediction of the liquid fraction, thereby allowing mixed-phase particles (Cholette et al., 2019, 2023). This improves the representation of several important processes including the partial melting of ice and their refreezing to form IP: both processes having significant impacts on simulations of a major FR event that occurred over eastern Canada and the United States (Cholette et al., 2020).

A recent focus of cloud physics research has been on processes involving secondary ice production (SIP), which is the generation of small ice crystals in concentrations exceeding those of primary ice nucleating particles at temperatures above the homogeneous freezing threshold (Field et al., 2017; Korolev & Leisner, 2020; Korolev et al., 2020). Several SIP mechanisms have been proposed, such as rime splintering (Hallett & Mossop, 1974), fragmentation of frozen drops (e.g., Mason & Maybank, 1960), sublimation fragmentation (Bacon et al., 1998) and collisional fragmentation (Takahashi et al., 1995; Vardiman, 1978). However, many of these remain poorly quantified. Recent modeling studies have demonstrated the importance of SIP for convective cases, where SIP leads to increased ice concentrations and mass contents aloft (e.g., Hou et al., 2023; Hua et al., 2023; Huang et al., 2021; Qu et al., 2022) and accelerated cloud glaciation (e.g., Connolly et al., 2006; Lawson et al., 2015; Miltenberger et al., 2020; Phillips et al., 2005; Sullivan et al., 2017). However, there have been fewer studies of SIP impacts on stratiform clouds or in winter storm cases, and, to our knowledge, no studies examining the impacts of SIP on FR. The focus of studies on SIP in stratiform clouds to date has been on orographic mixed-phase clouds (e.g., Dedekind et al., 2021; Georgakaki et al., 2022), polar mixed-phase clouds (Sotiropoulou et al., 2020; Zhao et al., 2021), cold frontal rainbands (Sullivan et al., 2018), cold marine boundary layer clouds (Karalis et al., 2022), and stratiform clouds globally (Zhao & Liu, 2021). In this study, we examine the impacts of including the *Hallett-Mossop* (HM) rime splintering SIP process on the simulation of FR using various configurations of the P3 scheme.

2. Methods

2.1. Description of the Simulations

All simulations were performed using the Global Environmental Multiscale (GEM) atmospheric model (Côté et al., 1998; Girard et al., 2014) with a configuration based on the operational HRDPS. The horizontal domain covers most of Canada and the northern US (Figure S1 in Supporting Information S1) with a horizontal grid spacing of 0.0225° (~ 2.5 km). The vertical grid consists of 62 staggered levels with the lowest thermodynamic level at ~ 20 m above ground level. The time step is 60 s and the forecast period for each case is 48 hr. In addition to the P3 microphysics scheme, the physical parameterizations include the Kain and Fritsch (1990, 1993) deep convection scheme, the Kuo-Transient shallow convection scheme (Bélair et al., 2005), and the Interaction Soil Biosphere Atmosphere land surface scheme (Bélair et al., 2003, 2005). Boundary layer turbulent mixing is based on a prognostic turbulent kinetic energy approach and a statistical representation of subgrid-scale clouds (Bélair et al., 2005; Benoit et al., 1989; Delage, 1988a, 1988b). The Li and Barker (2005) correlated k-distribution method is used to compute radiative transfer every 15 min.

The version of P3 used in this study predicts cloud and rain number and mass mixing ratios and 5 mixing ratio variables for each ice-phase (or mixed-phase) category: mass from riming, mass from vapor deposition, total number, rime volume, and liquid mass. The ice-phase categories are referred to as “free” as each is able to evolve continuously and represent any type of ice-phase hydrometeor (Milbrandt & Morrison, 2016). This

contrasts with traditional schemes using multiple pre-defined (fixed) categories. In P3, ice can grow by vapor deposition and further by riming, as all ice categories, including categories that are initiated via SIP, use the same growth equations. Details on the parameterized growth processes are given in SI (and in Cholette et al., 2019; Morrison & Milbrandt, 2015). We study the impact of including SIP using either one or two ice-phase categories, where $nCat$ denotes the number of categories. With $nCat > 1$, P3 can represent different modes/types of ice at the same time and location. This reduces the dilution of particle properties that may occur using $nCat = 1$ when, for example, small ice particles are produced in a grid volume by SIP in which large ice is already present. We examine the impacts of SIP through the *HM* rime splintering process (hereafter *HM*). *HM* is relatively well quantified compared to other SIP mechanisms, with the production of ice splinters (with an assumed diameter of 10 μm) occurring between -3°C and -8°C from accretion of large drops (rain) onto large, rimed ice particles. Details of the implementation of *HM* are given in the Supporting Information S1, as well as further details of the P3 scheme.

Four configurations of the model are analyzed (Table S1 in Supporting Information S1). The first is the baseline configuration of P3: one ice category and the *HM* process off ($nCat1_noHM$). The second has two ice categories and includes *HM* ($nCat2_HM$). The third and fourth are sensitivity runs: $nCat = 1$ with *HM* on ($nCat1_HM$) and $nCat = 2$ with *HM* off ($nCat2_noHM$).

2.2. Analysis

An analysis was conducted for the 27 February 2020 winter storm case that occurred over eastern Canada. There is a considerable over-prediction of explicit FR for this case in the region where snow was observed. This exemplifies a systematic problem in forecasts of winter explicit precipitation types using the operational HRDPS. Over the Maritime provinces, the 48-hr accumulated total precipitation from the simulations is compared to ERA5 (Hersbach et al., 2020) and Canadian Precipitation Analysis (CaPA) observations (Khedhaouiria et al., 2020; Lespinas et al., 2015; Mahfouf et al., 2007). The precipitation types (for total hourly accumulation >0.1 mm) are compared to hourly surface observations at six representative weather stations (<https://weather.uwyo.edu/surface/>). The precipitation types considered are snow, IP, FR and rain. In the simulations, the distinction between rain (when $T_{kbot} \geq 0^{\circ}\text{C}$) and FR (when $T_{kbot} < 0^{\circ}\text{C}$) is based on the temperature at the lowest model level (T_{kbot}). “Rain” and “Freezing rain” in this study include both drizzle (small drops) and rain (large drops) for the observations and simulations; the only observed reports of drizzle for this case were during a 3-hr period at YHZ. This also avoids the problem of having to apply an ad-hoc size threshold to differentiate between drizzle and rain in the simulations. When the bulk ice from the model has a rimed mass fraction >0.5 and a rime mass density >750 kg m^{-3} , it is assumed to be IP; otherwise, it is considered snow (more details in SI).

Forecast skill scores for the occurrence of rain, FR, and snow are examined for a set of 40 winter cases during January and February 2020. The analyzed scores (defined in SI) are the frequency bias index (FBI) and the equitable threat score (ETS). The false alarm ratio (FAR) and the probability of detection (POD) are also analyzed (SI). Explicit simulations of precipitation type are compared to the Bourgozin (2000) diagnostic algorithm, currently used to determine the precipitation type in the operational HRDPS. The Bourgozin algorithm is applied to temperature and relative humidity profiles from the baseline $nCat1_noHM$ simulations and will be referred to as $nCat1_noHM_Bourgozin$. Similar results are obtained applying Bourgozin to simulations from the other configurations since the thermodynamic profiles vary little among them. We focus on scores for FR; scores for rain and snow are very similar among the runs (Figures S10 and S11 in Supporting Information S1). Scores for IP are not shown because the number of observed cases was too small.

3. Results

3.1. The 27 February 2020 Case

At the model initialization time (00 UTC 27 February 2020), there was a low surface pressure of 975 hPa near the border between Virginia and Kentucky with a surface pressure gradient along the North American east coast. The surface low was nearly aligned with a 500 hPa geopotential height low. Surface temperatures were between -10°C and 2°C over the Maritime provinces with the 0°C isotherm across central New Brunswick and Nova Scotia. After 24 hr, the system moved slowly over the Maritimes, while the 0°C isotherm remained approximately over the same location and the surface low was still nearly aligned with the 500 hPa low. Maximum total precipitation

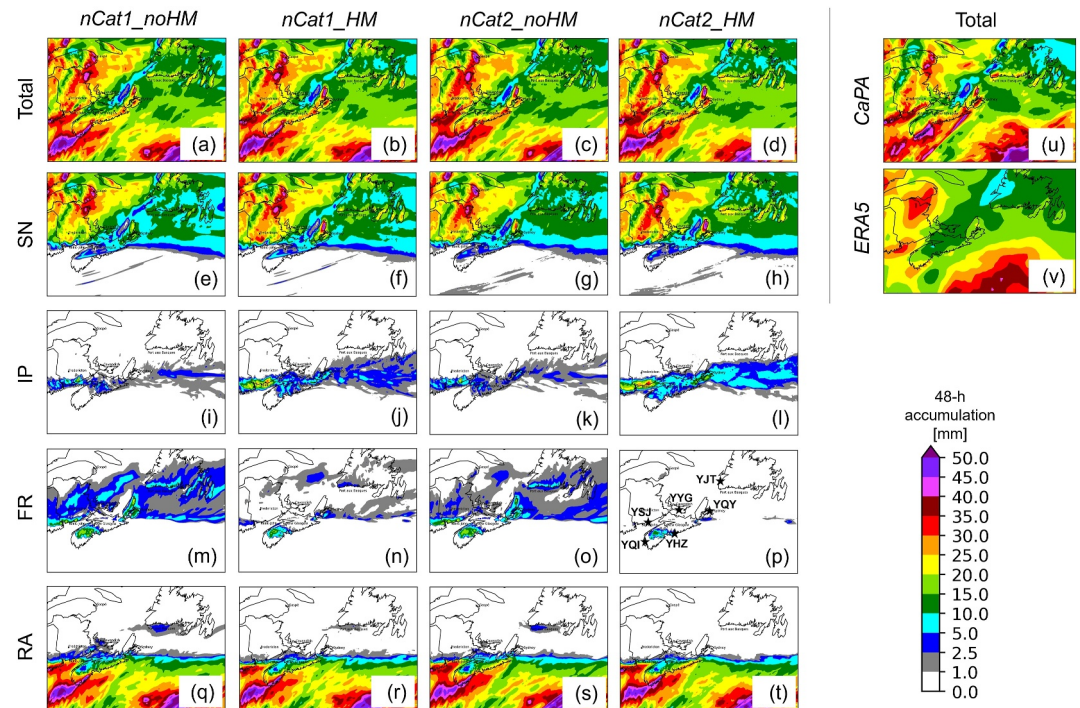


Figure 1. 48-h accumulation (liquid equivalent) [mm] ending at 00 UTC 29 February 2020 of (a)–(d) total precipitation, (e)–(h) snow (SN), (i–l) ice pellets, (m–p) freezing rain and (q–t) rain (RA) from (a, e, i, m, q) *nCat1_noHM*, (b, f, j, n, r) *nCat1_HM*, (c, g, k, o, s) *nCat2_noHM*, and (d, h, l, p, t) *nCat2_HM*, and (u–v) total precipitation from (u) Canadian Precipitation Analysis and (v) ERA5. Locations of the 6 stations in Figure 2 are shown in panel (p).

accumulation (~50 mm) occurred near the east coast of Nova Scotia and the Gaspé Peninsula (Figures 1u and 1v). The total precipitation in all simulations generally compares well with CaPA (Figures 1a–1d), with an overestimation of 5–10 mm over the east coast of New Brunswick and southern Nova Scotia, and an underestimation of 10–15 mm over the ocean in the south-east portion of the domain. Total precipitation amounts are increased by less than 3% for the two simulations with $nCat = 2$ (*nCat2_HM* and *nCat2_noHM*) compared to the control simulation (*nCat1_noHM*) over the analysis domain, with similar spatial distributions.

A transition from mostly rain in the southern part of the domain to snow in the north occurs in all simulations consistent with the observations (Figures 1e–1t), with precipitation starting earlier in the south than in the north (Figure 2). Rain is produced in the south (Figures 1q–1t) because the surface temperature remains above 0°C. A mixture of precipitation types was observed between the northern and southern weather stations (Figures 1e–1p and 2c–2l). The precipitation type transition is generally well simulated by all simulations (Figure 2 and Figure S3 in Supporting Information S1). At all stations, FR was mainly observed when the temperature profiles had a melting layer aloft and a subfreezing layer near the surface. Further north, IP were not observed, yet they are simulated (Figures 2c and 2d).

The main difference between the observed and simulated precipitation types in *nCat1_noHM* is the overestimation of FR in regions where the entire tropospheric temperature profile is below 0°C (i.e., no melting layer aloft) or when the melting layer is very shallow (Figures S6–S8 in Supporting Information S1). For example, at the northern station (YJT), the observed and simulated temperature profiles remain below 0°C for the entire event; only snow was observed. *nCat2_HM* gives mostly snow which is consistent with the observations (Figure 2b), but *nCat1_noHM* gives a mixture of snow and FR (Figure 2a). The overestimation of FR over the northern portion of the domain (i.e., at YJT) also occurs with *nCat2_noHM*, but is reduced in *nCat1_HM* (Figures 1n and 1o). The FR in the region originates from liquid-phase processes including autoconversion of cloud droplets to rain and accretion of cloud water by rain (Figure S4 in Supporting Information S1). The importance of autoconversion in driving this excessive FR is further illustrated by a sensitivity test using *nCat1_HM* but with autoconversion shut off (*nCat1_HM_noauto*). Freezing rain is substantially reduced in this simulation, especially in the northern part

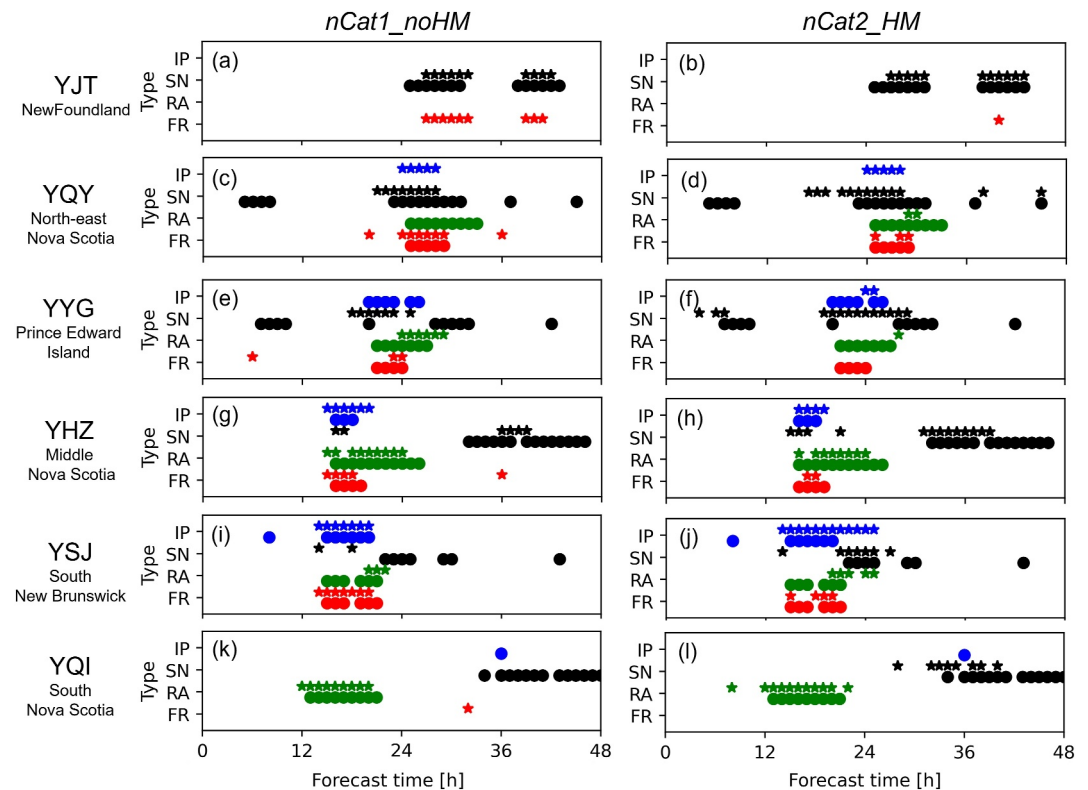


Figure 2. Time series of hourly precipitation type (black is snow (SN), green is rain (RA), red is freezing rain, and blue is ice pellets) from METARs at each station (circle) and the model (stars) for (a, c, e, g, i) *nCat1_noHM* and (b, d, f, h, j) *nCat2_HM* at stations (a)–(b) YJT, (c)–(d) YQY, (e)–(f) YYG, (g)–(h) YHZ, (i)–(j) YSJ, and (k)–(l) YQI. Locations of the stations are shown in Figure 1p. Only hours with total precipitation (liquid equivalent) > 0.1 mm are shown.

of the domain (Figure S2i in Supporting Information S1). The bias in FR using *nCat1_HM* is insensitive to details of the autoconversion parameterization; an additional test using the Kogan (2013) parameterization instead of Khairoutdinov and Kogan (2000) in the baseline model produces similar results of accumulated precipitation types as *nCat1_HM* (not shown).

For both *nCat* = 1 and *nCat* = 2, simulations with *HM* reduce the occurrence (Figure 2) and spatial coverage (Figures 1n and 1p) of FR, especially in the north, and increase IP and snow (Figures 1j and 1l and Figures S2f, S2h, S2j, S2l in Supporting Information S1). *nCat2_HM* is closer to the METAR reports of precipitation type, except over Prince Edward Island (YYG in Figure 2). Although similar overall total precipitation accumulation is obtained in the simulations, the relative reduction of FR accumulation is 65% and 98% for the *HM* compared to *noHM* simulations for *nCat* = 1 and *nCat* = 2, and the relative increase in ice pellet accumulation is 95% and 120%, respectively.

Simulations with *HM* reduce the FR accumulation in regions where rime splintering is active. Results are consistent at different analysis times as seen by the cross-sections in Figure 3 and Figure S4–S8 in Supporting Information S1. Note that the cross-section (Figures S6–S8 in Supporting Information S1) at 31 hr simulation time has a prominent elevated melting layer aloft, while the second cross-section at 33 hr (Figure 3 and Figures S4–S5 in Supporting Information S1) does not. Differences between the *HM* and *noHM* simulations occur mainly at low levels (below 4 km) where cloud and rain are present, primarily between 200 and 350 km horizontally along both cross-sections. It is clear that rime splintering plays a key role in reducing FR in this 200–350 km region. It has less impact with *nCat1_HM* than with *nCat2_HM* in general, but a reduction of FR still occurs in *nCat1_HM* (Figure 3x and Figure S6x in Supporting Information S1). With *noHM*, cloud water converts to rain through autoconversion, which grow further by accretion of cloud. With limited ice present in these regions, this supercooled rain falls to the surface as FR.

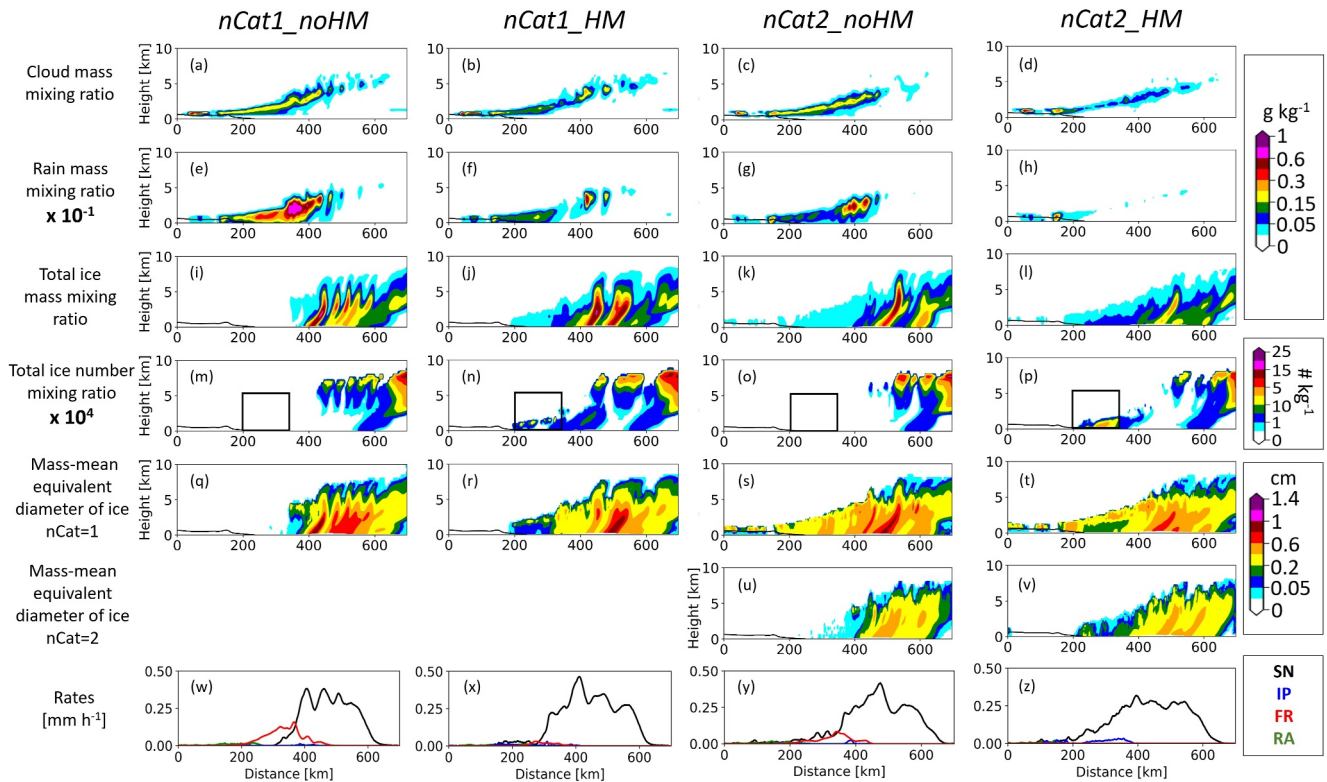


Figure 3. Averaged vertical cross-sections of various quantities over the region within the blue box of Figure S1 in Supporting Information S1 at 33 hr forecast time: (a)–(d) cloud mass mixing ratio [g kg^{-1}], (e)–(h) rain mass mixing ratios [g kg^{-1}], (i)–(l) total ice mass mixing ratios [g kg^{-1}], (m)–(p) total ice number mixing ratios [$\# \text{kg}^{-1}$], and (q)–(v) ice mass-mean equivalent diameter [cm] of (q)–(t) category #1 and (u)–(v) category #2. Also shown are (w)–(z) hourly accumulation [mm h^{-1}] of snow (SN; black), ice pellets (IP; blue), freezing rain (FR; red) and rain (RA; green). Results are presented for (a, e, i, m, q, w) *nCat1_noHM*, (b, f, j, n, r, x) *nCat1_HM*, (c, g, k, o, s, u, y) *nCat2_noHM*, and (d, h, l, p, t, v, z) *nCat2_HM*. The y-axis is height and the x-axis is horizontal distance from southwest to northeast along the length (longer dimension) of the rectangular blue box in Figure S1 in Supporting Information S1, while horizontal averaging is applied along its width (shorter dimension). The black lines in panels (a)–(v) are the 0°C -isotherm. The black squares in panels (m)–(p) show the region over which the % difference (*Hallett-Mossop-noHM*) in the process rates are analyzed.

With *HM*, new ice particles are produced by rime splintering, and they grow by vapor deposition and riming. Correspondingly, simulations with *HM* have greater ice mass (Figures 3j and 3l and Figures S6j and S6l in Supporting Information S1) and number (Figures 3n and 3p and Figures S6n and S6p in Supporting Information S1) where *HM* is active than without *HM*, particularly for *nCat2_HM*. Below, the numbers in parentheses (expressed in % range between *nCat1* and *nCat2* simulations) are the relative differences between *HM* and *noHM* averaged over the two cross-sections from 200 to 350 km horizontally and 0–5 km vertically (boxes shown in Figures 3m–3p). Reductions of several liquid-phase process rates, including cloud condensation (–22% to –58%), autoconversion (–46% to –82%), cloud accretion by rain (–55% to –76%), rain condensation (–58% to –73%) and rain evaporation (–44% to –95%), occur with *HM* compared to *noHM* (Figures S4 and S7 in Supporting Information S1). This is a consequence of less cloud liquid and rain mass with the increase in ice number and mass owing to *HM*. Enhanced ice number associated with *HM* leads to an increased bulk deposition rate (+465–1,340%) in the region of rime splintering (Figures S5e–S5h and S8e–S8h in Supporting Information S1), which limits water vapor available for condensation. This also further reduces cloud water and rain by increasing mean ice particle size (Figures 3q–3v and Figures S6q–S6v in Supporting Information S1) and fall speed and hence increasing the collection kernel. Together with greater ice particle number, this leads to higher riming rates (+100 to 135%) on average in the simulations with *HM* compared to without in the analysis region. Riming rates are reduced for *nCat2_HM* at 33 hr simulation time compared to *nCat2_noHM* simply because there is little supercooled liquid water remaining by this time. It is concluded that the *HM* process leads to increased ice number and mass mixing ratios and enhanced depositional growth and riming efficiency which reduce supercooled cloud water and rain and hence FR accumulation for both *nCat* = 1 and *nCat* = 2, although the impacts are somewhat greater for *nCat* = 2.

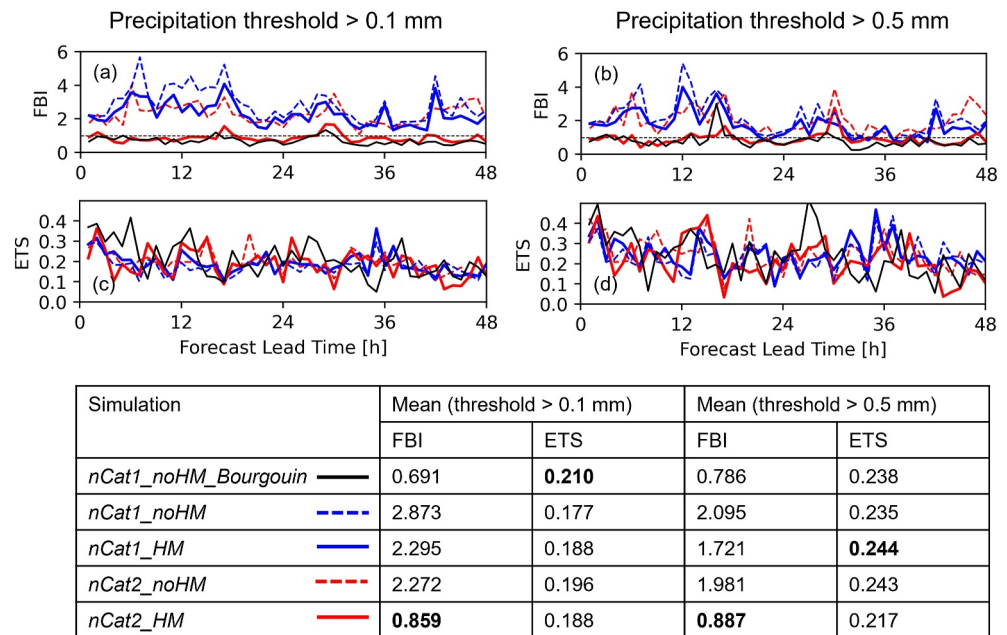


Figure 4. Freezing rain (a–b) frequency bias index and (c–d) equitable threat score skill scores for *nCat1_noHM* (dashed blue), *nCat2_HM* (solid red), *nCat1_HM* (solid blue), *nCat2_noHM* (dashed red), and *nCat1_noHM_Bourgouin* (black) (*nCat1_noHM* but with precipitation type determined by the diagnostic Bourgouin algorithm) for a series of 40 cases during January and February 2020 and for precipitation thresholds of (a and c) 0.1 mm and (b and d) 0.5 mm. Mean skill score values are listed in the table. Bold font in the table indicates simulations with the greatest skill.

3.2. Forecast Skill Scores for Precipitation Phase (40 Cases)

The FBI and ETS scores for two different FR accumulation thresholds (0.1 and 0.5 mm) are shown in Figure 4 for a series of 40 winter cases (including the case discussed above). Scores for total precipitation are similar among the simulations (not shown). POD and FAR scores are shown in SI. The FBI is substantially improved for FR with *HM* included compared to *noHM*, especially for *nCat2_HM* (with values of unity representing perfect skill). A reduced FBI with a neutral change in ETS represents a systematic statistical improvement (e.g., Murphy, 1996; Jolliffe, 2008). The FBI for FR from *nCat2_HM* is slightly better (closer to unity) compared to using the Bourgouin diagnostic, which is empirical and highly tuned, for both accumulation thresholds. ETS is more similar among the simulations, with maximum differences of 11%–17%. Both POD and FAR are reduced with *nCat2_HM* and are similar to *nCat1_noHM_Bourgouin* (Figure S9 in Supporting Information S1); note that perfect scores for POD and FAR are 1 and 0, respectively. The reduction of POD with *nCat2_HM* may indicate a too large reduction of occurrence of small amounts of FR; this will be investigated in future studies. In general, the skill scores for rain (Figure S10 in Supporting Information S1) and snow (Figure S11 in Supporting Information S1) are similar among all simulations, and better overall than those of FR.

4. Conclusions

Our results show that the Hallett-Mossop (*HM*) rime splintering mechanism of SIP has a critical impact on precipitation phase and type at the surface in winter storms. In the Canadian high-resolution (2.5 km) NWP system, including the parameterized *HM* process substantially reduced the occurrence of FR systematically and improved the simulation of precipitation type compared to observations, particularly using the two ice-phase categories configuration of the P3 microphysics scheme. Ice particles produced by rime splintering increased collection of supercooled rain and led to an increase of snow and ice pellet accumulation in regions where FR was incorrectly predicted by the model without *HM*. In addition to the influence of SIP on microphysical properties in deep convection as shown in past studies (e.g., Qu et al., 2022), our results indicate the importance of SIP in correctly simulating precipitation type for winter storms. Our results also suggest the potential for using the predicted hydrometeor properties to forecast winter precipitation types explicitly. For simulations using P3 with two ice-phase categories and including *HM*, the explicit approach gave comparable or slightly better skill scores

compared to an empirical, highly tuned diagnostic algorithm. These results are also relevant to climate model projections of winter precipitation type using physically based, explicit predictions of precipitation hydrometeor properties.

While the model results presented in this study with the *HM* process included are encouraging and show a systematic improvement in hindcast simulations of FR, one must keep in mind that laboratory studies of rime splintering and other SIP processes have several limitations (Korolev et al., 2020) and the reproducibility of the original experiments reported in Hallett and Mossop (1974) have been recently questioned (Seidel et al., 2023). Thus, model parameterizations of SIP based on past studies are uncertain. Nonetheless, our results demonstrate that accounting for SIP in the simulation can have a large beneficial impact on the explicit simulation of winter precipitation. In our simulations, the *HM* process increased the concentration of small ice particles, which in turn increased the bulk ice mass through vapor deposition and riming depleting the supercooled cloud water and rain and thereby reducing the FR at the surface. It is anticipated that other SIP processes leading to increased concentrations of small ice particles would have a similar impact following this chain of process interactions. The impacts of including different SIP mechanisms in simulations of winter precipitation types will be explored in future work. Uncertainty in parameterizations of SIP also points to the need for continued research (e.g., laboratory experiments and in-situ observation campaigns) into the fundamental physics behind these natural processes to improve their representation in models.

Data Availability Statement

The code for the P3 microphysics scheme is available on <https://github.com/P3-microphysics/P3-microphysics/>. The GEM model code is available on <https://github.com/ECCC-ASTD-MRD/gem>. All data including those used to initialize the simulations, the simulated outputs, the Python plotting scripts and the CaPA product (Khedhaouiria et al., 2020; Lespinas et al., 2015; Mahfouf et al., 2007) used in this study are archived internally for 5-year at the Canadian Meteorological Centre. METAR data from the University of Wyoming web site (<http://weather.uwyo.edu/>) and ERA5 is available on <https://confluence.ecmwf.int/display/CKB/How+to+download+ERA5> (Hersbach et al., 2020).

Acknowledgments

The first author would like to thank Paul Vaillancourt, Ayrton Zadra, Danahé Paquin-Ricard, Ron McTaggart-Cowan, Barbara Casati, Marc Verville and Zhipeng Qu of Environment and Climate Change Canada for their help and discussions of the results.

References

- Bacon, N. J., Swanson, B. D., Baker, M. B., & Davis, E. J. (1998). Breakup of levitated frost particles. *Journal of Geophysical Research*, 103(13), 763–775. <https://doi.org/10.1029/98JD01162>
- Barszcz, A., Milbrandt, J. A., & Thériault, J. M. (2018). Improving the explicit prediction of freezing rain in a kilometer-scale numerical weather prediction model. *Weather and Forecasting*, 33(3), 767–782. <https://doi.org/10.1175/WAF-D-17-0136.1>
- Bélair, S., Crevier, L. P., Mailhot, J., Bilodeau, B., & Delage, Y. (2003). Operational implementation of the ISBA land surface scheme in the Canadian regional weather forecast model. Part I: Warm season results. *Journal of Hydrometeorology*, 4(2), 352–370. [https://doi.org/10.1175/1525-7541\(2003\)4<352:OITOL>2.0.CO;2](https://doi.org/10.1175/1525-7541(2003)4<352:OITOL>2.0.CO;2)
- Bélair, S., Mailhot, J., Girard, C., & Vaillancourt, P. (2005). Boundary layer and shallow cumulus clouds in a medium-range forecast of a large-scale weather system. *Monthly Weather Review*, 133(7), 1938–1960. <https://doi.org/10.1175/MWR2958.1>
- Benoit, R., Côté, J., & Mailhot, J. (1989). Inclusion of a TKE boundary layer parameterization in the Canadian regional finite-element model. *Monthly Weather Review*, 117(8), 1726–1750. [https://doi.org/10.1175/1520-0493\(1989\)117<1726:IOATBL>2.0.CO;2](https://doi.org/10.1175/1520-0493(1989)117<1726:IOATBL>2.0.CO;2)
- Bourgouin, P. (2000). A method to determine precipitation types. *Weather and Forecasting*, 15(5), 583–592. [https://doi.org/10.1175/1520-0434\(2000\)015<0583:AMTDPT>2.0.CO;2](https://doi.org/10.1175/1520-0434(2000)015<0583:AMTDPT>2.0.CO;2)
- Bresson, É., Laprise, R., Paquin, D., Thériault, J. M., & de Elía, R. (2017). Evaluating the ability of CRCM5 to simulate mixed precipitation. *Atmosphere-Ocean*, 55(2), 79–93. <https://doi.org/10.1080/07055900.2017.1310084>
- Caron, J.-F., Jacques, D., Paquin-Ricard, D., Faucher, M., Milewski, T., & Verville, M. (2021). *High resolution deterministic prediction system – National domain (HRDPS-NAT)*. Update from version 5.2.0 to version 6.0.0 (p. 45). Technical Note, Canadian Meteorological Centre.
- Chang, S. E., McDaniels, T. L., Mikawoz, J., & Peterson, K. (2007). Infrastructure failure interdependencies in extreme events: Power outage consequences in the 1998 Ice Storm. *Natural Hazards*, 41(2), 337–358. <https://doi.org/10.1007/s11069-006-9039-4>
- Cheng, C. S., Auld, H., Li, G., Klaassen, J., & Li, Q. (2007). Possible impacts of climate change on freezing rain in south-central Canada using downscaled future climate scenarios. *Natural Hazards and Earth System Sciences*, 7(1), 71–87. <https://doi.org/10.5194/nhess-7-71-2007>
- Cheng, C. S., Li, G., & Auld, H. (2011). Possible impacts of climate change on freezing rain using downscaled future climate scenarios: Updated for Eastern Canada. *Atmosphere-Ocean*, 49(1), 8–21. <https://doi.org/10.1080/07055900.2011.555728>
- Cholette, M., Milbrandt, J. A., Morrison, H., Paquin-Ricard, D., & Jacques, D. (2023). Combining triple-moment ice with prognostic liquid fraction in the P3 microphysics scheme: Impacts on a simulated squall line. *Journal of Advances in Modeling Earth Systems*, 15(4), e2022MS003328. <https://doi.org/10.1029/2022MS003328>
- Cholette, M., Morrison, H., Milbrandt, J. A., & Thériault, J. M. (2019). Parameterization of the bulk liquid fraction on mixed-phase particles in the predicted particle properties (P3) scheme: Description and idealized simulations. *Journal of the Atmospheric Sciences*, 76(2), 561–582. <https://doi.org/10.1175/JAS-D-18-0278.1>
- Cholette, M., Thériault, J. M., Milbrandt, J. A., & Morrison, H. (2020). Impacts of predicting the liquid fraction of mixed-phase particles on the simulation of an extreme freezing rain event: The 1998 North American Ice Storm. *Monthly Weather Review*, 148(9), 3799–3823. <https://doi.org/10.1175/MWR-D-20-0026.1>

- Connolly, P. J., Heymsfield, A. J., & Choulaton, T. W. (2006). Modelling the influence of rimer surface temperature on the glaciation of intense thunderstorms: The rime-splinter mechanism of ice multiplication. *Quarterly Journal of the Royal Meteorological Society: A Journal of the Atmospheric Sciences, Applied Meteorology and Physical Oceanography*, 132(621C), 3059–3077. <https://doi.org/10.1256/qj.05.45>
- Cortinas Jr, J. V., Bernstein, B. C., Robbins, C. C., & Strapp, J. W. (2004). An analysis of freezing rain, freezing drizzle, and ice pellets across the United States and Canada: 1976–90. *Weather and Forecasting*, 19(2), 377–390. [https://doi.org/10.1175/1520-0434\(2004\)019<0377:AAOFRF>2.0.CO;2](https://doi.org/10.1175/1520-0434(2004)019<0377:AAOFRF>2.0.CO;2)
- Côté, J., Gravel, S., Méthot, A., Patoine, A., Roch, M., & Staniforth, A. (1998). The operational CMC–MRB global environmental multiscale (GEM) model. Part I: Design considerations and formulation. *Monthly Weather Review*, 126(6), 1373–1395. [https://doi.org/10.1175/1520-0493\(1998\)126<1373:TOCMGE>2.0.CO;2](https://doi.org/10.1175/1520-0493(1998)126<1373:TOCMGE>2.0.CO;2)
- Dedekind, Z., Lauber, A., Ferrachat, S., & Lohmann, U. (2021). Sensitivity of precipitation formation to secondary ice production in winter orographic mixed-phase clouds. *Atmospheric Chemistry and Physics*, 21(19), 15115–15134. <https://doi.org/10.5194/acp-21-15115-2021>
- Delage, Y. (1988a). The position of the lowest levels in the boundary layer of atmospheric circulation models. *Atmosphere-Ocean*, 26(3), 329–340. <https://doi.org/10.1080/07055900.1988.9649307>
- Delage, Y. (1988b). A parameterization of the stable atmospheric boundary layer. *Boundary-Layer Meteorology*, 43(4), 365–381. <https://doi.org/10.1007/BF00121713>
- Elmore, K. L., Grams, H. M., Apps, D., & Reeves, H. D. (2015). Verifying forecast precipitation type with mPING. *Weather and Forecasting*, 30(3), 656–667. <https://doi.org/10.1175/WAF-D-14-00068.1>
- Field, P. R., Lawson, R. P., Brown, P. R., Lloyd, G., Westbrook, C., Moiseev, D., et al. (2017). Secondary ice production: Current state of the science and recommendations for the future. *Meteorological Monographs*, 58, 7-1. <https://doi.org/10.1175/AMSMONOGRAPH5-D-16-0014.1>
- Frick, C., Seifert, A., & Wernli, H. (2013). A bulk parametrization of melting snowflakes with explicit liquid water fraction for the COSMO model. *Geoscientific Model Development*, 6(6), 1925–1939. <https://doi.org/10.5194/gmd-6-1925-2013>
- Georgakaki, P., Sotiropoulou, G., Vignon, É., Billault-Roux, A. C., Berne, A., & Nenes, A. (2022). Secondary ice production processes in wintertime alpine mixed-phase clouds. *Atmospheric Chemistry and Physics*, 22(3), 1965–1988. <https://doi.org/10.5194/acp-22-1965-2022>
- Girard, C., Plante, A., Desgagné, M., McTaggart-Cowan, R., Côté, J., Charron, M., et al. (2014). Staggered vertical discretization of the Canadian Environmental Multiscale (GEM) model using a coordinate of the log-hydrostatic-pressure type. *Monthly Weather Review*, 142(3), 1183–1196. <https://doi.org/10.1175/MWR-D-13-00255.1>
- Hallett, J., & Mossop, S. C. (1974). Production of secondary ice particles during the riming process. *Nature*, 249(5452), 26–28. <https://doi.org/10.1038/249026a0>
- Hersbach, H., Bell, B., Berrisford, P., Hirahara, S., Horányi, A., Muñoz-Sabater, J., et al. (2020). The ERA5 global reanalysis [Dataset]. *Quarterly Journal of the Royal Meteorological Society*, 146(730), 1999–2049. <https://doi.org/10.1002/qj.3803>
- Hou, T., Chen, B., Lei, H., Wei, L., He, Y., & Feng, Q. (2023). Evaluation of the predicted particle properties (P3) microphysics scheme in simulations of stratiform clouds with embedded convection. *Advances in Atmospheric Sciences*, 40(10), 1–18. <https://doi.org/10.1007/s00376-023-2178-7>
- Hua, S., Chen, B., Liu, Y., Chen, G., Yang, Y., Dong, X., et al. (2023). Evaluation of the ice particle simulation of microphysics schemes with aircraft measurements of a stratiform cloud in North China. *Journal of the Atmospheric Sciences*, 80(6), 1635–1656. <https://doi.org/10.1175/JAS-D-22-0155.1>
- Huang, Y., Wu, W., McFarquhar, G. M., Wang, X., Morrison, H., Ryzhkov, A., et al. (2021). Microphysical processes producing high ice water contents (HIWCs) in tropical convective clouds during the HAIC-HIWC field campaign: Evaluation of simulations using bulk microphysical schemes. *Atmospheric Chemistry and Physics*, 21(9), 6919–6944. <https://doi.org/10.5194/acp-21-6919-2021>
- Jolliffe, I. T. (2008). The impenetrable hedge: A note on propriety, equitability and consistency. *Meteorological Applications: A Journal of Forecasting, Practical Applications, Training Techniques and Modelling*, 15(1), 25–29. <https://doi.org/10.1002/met.60>
- Kain, J. S., & Fritsch, J. M. (1990). A one-dimensional entraining/detraining plume model and its application in convective parameterization. *Journal of the Atmospheric Sciences*, 47(23), 2784–2802. [https://doi.org/10.1175/1520-0469\(1990\)047<2784:AODEPM>2.0.CO;2](https://doi.org/10.1175/1520-0469(1990)047<2784:AODEPM>2.0.CO;2)
- Kain, J. S., & Fritsch, J. M. (1993). Convective parameterization for mesoscale models: The Kain-Fritsch scheme. In K. A. Emanuel & D. J. Raymond (Eds.), *The representation of cumulus convection in numerical models. Meteorological monographs*. American Meteorological Society. https://doi.org/10.1007/978-1-935704-13-3_16
- Karalis, M., Sotiropoulou, G., Abel, S. J., Bossioli, E., Georgakaki, P., Methymaki, G., et al. (2022). Effects of secondary ice processes on a stratocumulus to cumulus transition during a cold-air outbreak. *Atmospheric Research*, 277, 106302. <https://doi.org/10.1016/j.atmosres.2022.106302>
- Khedhaouria, D., Bélair, S., Fortin, V., Roy, G., & Lespinas, F. (2020). High-resolution (2.5 km) ensemble precipitation analysis across Canada. *Journal of Hydrometeorology*, 21(9), 2023–2039. <https://doi.org/10.1175/JHM-D-19-0282.1>
- King, S., & Laplante, D. P. (2005). The effects of prenatal maternal stress on children's cognitive development: Project Ice Storm. *Stress: The International Journal on the Biology of Stress*, 8(1), 35–45. <https://doi.org/10.1080/10253890500108391>
- Kogan, Y. (2013). A cumulus cloud microphysics parameterization for cloud-resolving models. *Journal of the Atmospheric Sciences*, 70(5), 1423–1436. <https://doi.org/10.1175/JAS-D-12-0183.1>
- Korolev, A., Heckman, I., Wolde, M., Ackerman, A. S., Fridlind, A. M., Ladino, L. A., et al. (2020). A new look at the environmental conditions favorable to secondary ice production. *Atmospheric Chemistry and Physics*, 20(3), 1391–1429. <https://doi.org/10.5194/acp-20-1391-2020>
- Korolev, A., & Leisner, T. (2020). Review of experimental studies of secondary ice production. *Atmospheric Chemistry and Physics*, 20(20), 11767–11797. <https://doi.org/10.5194/acp-20-11767-2020>
- Lambert, S. J., & Hansen, B. K. (2011). Simulated changes in the freezing rain climatology of North America under global warming using a coupled climate model. *Atmosphere-Ocean*, 49(3), 289–295. <https://doi.org/10.1080/07055900.2011.607492>
- Lawson, R. P., Woods, S., & Morrison, H. (2015). The microphysics of ice and precipitation development in tropical cumulus clouds. *Journal of the Atmospheric Sciences*, 72(6), 2429–2445. <https://doi.org/10.1175/JAS-D-14-0274.1>
- Lecompte, E. L., Russell, J. W., & Pang, A. W. (1998). La tempête de verglas de 1998. *Institut de Prévention des Sinistres Catastrophiques Tech. Rep.*, 45. Retrieved from https://www.iclr.org/wpcontent/uploads/PDFS/1998_ice_storm_report_french.pdf
- Lespinas, F., Fortin, V., Roy, G., Rasmussen, P., & Stednyk, T. (2015). Performance evaluation of the Canadian precipitation analysis (CaPA). *Journal of Hydrometeorology*, 16(5), 2045–2064. <https://doi.org/10.1175/JHM-D-14-0191.1>
- Li, J., & Barker, H. W. (2005). A radiation algorithm with correlated-k distribution. Part I: Local thermal equilibrium. *Journal of the Atmospheric Sciences*, 62(2), 286–309. <https://doi.org/10.1175/JAS-3396.1>

- Mahfouf, J. F., Brasnett, B., & Gagnon, S. (2007). A Canadian precipitation analysis (CaPA) project: Description and preliminary results. *Atmosphere-Ocean*, 45(1), 1–17. <https://doi.org/10.3137/ao.v450101>
- Manikin, G. S., Brill, K. F., & Ferrier, B. (2004). An Eta Model precipitation type mini-ensemble for winter weather forecasting. In *20th conf. On weather analysis and forecasting/16th conf. On numerical weather prediction*, Seattle, WA (Vol. 23.1). American Meteorological Society. Retrieved from <https://ams.confex.com/ams/pdfpapers/73517.pdf>
- Mason, B. J., & Maybank, J. (1960). The fragmentation and electrification of freezing water drops. *Quarterly Journal of Royal Meteorological Society*, 86(368), 176–185. <https://doi.org/10.1002/qj.49708636806>
- Matte, D., Thériault, J. M., & Laprise, R. (2018). Mixed precipitation occurrences over southern Québec, Canada, under warmer climate conditions using a regional climate model. *Climate Dynamics*, 53(1–2), 1–17. <https://doi.org/10.1007/s00382-018-4231-2>
- McCray, C. D., Atallah, E. H., & Gyakum, J. R. (2019). Long-duration freezing rain events over North America: Regional climatology and thermodynamic evolution. *Weather and Forecasting*, 34(3), 665–681. <https://doi.org/10.1175/WAF-D-18-0154.1>
- Milbrandt, J. A., Bélair, S., Faucher, M., Vallée, M., Carrera, M. L., & Glazer, A. (2016). The pan-Canadian high resolution (2.5 km) deterministic prediction system. *Weather and Forecasting*, 31(6), 1791–1816. <https://doi.org/10.1175/WAF-D-16-0035.1>
- Milbrandt, J. A., & Morrison, H. (2016). Parameterization of cloud microphysics based on the prediction of bulk ice particle properties. Part III: Introduction of multiple free categories. *Journal of the Atmospheric Sciences*, 73(3), 975–995. <https://doi.org/10.1175/JAS-D-15-0204.1>
- Miltenberger, A. K., Lüttmer, T., & Siewert, C. (2020). Secondary ice formation in idealised deep convection—Source of primary ice and impact on glaciation. *Atmosphere*, 11(5), 542. <https://doi.org/10.3390/atmos11050542>
- Morrison, H., Curry, J. A., & Khvorostyanov, V. I. (2005). A new double-moment microphysics parameterization for application in cloud and climate models. Part I: Description. *Journal of the Atmospheric Sciences*, 62(6), 1665–1677. <https://doi.org/10.1175/JAS3446.1>
- Morrison, H., & Milbrandt, J. A. (2015). Parameterization of cloud microphysics based on the prediction of bulk ice particle properties. Part I: Scheme description and idealized tests. *Journal of the Atmospheric Sciences*, 72(1), 287–311. <https://doi.org/10.1175/JAS-D-14-0065.1>
- Murphy, A. H. (1996). The Finley affair: A signal event in the history of forecast verification. *Weather and Forecasting*, 11(1), 3–20. [https://doi.org/10.1175/1520-0434\(1996\)011<0003:TFAASE>2.0.CO;2](https://doi.org/10.1175/1520-0434(1996)011<0003:TFAASE>2.0.CO;2)
- Phillips, V. T., Andronache, C., Sherwood, S. C., Bansemer, A., Conant, W. C., Demott, P. J., et al. (2005). Anvil glaciation in a deep cumulus updraught over Florida simulated with the Explicit Microphysics Model. I: Impact of various nucleation processes. *Quarterly Journal of the Royal Meteorological Society: A Journal of the Atmospheric Sciences, Applied Meteorology and Physical Oceanography*, 131(609), 2019–2046. <https://doi.org/10.1256/qj.04.85>
- Qu, Z., Korolev, A., Milbrandt, J. A., Heckman, I., Huang, Y., McFarquhar, G. M., et al. (2022). The impacts of secondary ice production on microphysics and dynamics in tropical convection. *Atmospheric Chemistry and Physics*, 22(18), 12287–12310. <https://doi.org/10.5194/acp-22-12287-2022>
- Ralph, F. M., Rauber, R. M., Jewett, B. F., Kingsmill, D. E., Pisano, P., Pugnier, P., et al. (2005). Improving short-term (0–48 h) cool-season quantitative precipitation forecasting: Recommendations from a USWRP workshop. *Bulletin of the American Meteorological Society*, 86(11), 1619–1632. <https://doi.org/10.1175/bams-86-11-1619>
- Reeves, H. D., Elmore, K. L., Ryzhkov, A., Schuur, T., & Krause, J. (2014). Sources of uncertainty in precipitation-type forecasting. *Weather and Forecasting*, 29(4), 936–953. <https://doi.org/10.1175/WAF-D-14-00007.1>
- Reeves, H. D., Ryzhkov, A. V., & Krause, J. (2016). Discrimination between winter precipitation types based on spectral-bin microphysical modeling. *Journal of Applied Meteorology and Climatology*, 55(8), 1747–1761. <https://doi.org/10.1175/JAMC-D-16-0044.1>
- Seidel, J. S., Kiselev, A., Keinert, A., Stratmann, F., Leisner, T., & Hartmann, S. (2023). Secondary ice production—No evidence of efficient rime-splintering mechanism. *EGU sphere*, 2023, 1–39. <https://doi.org/10.5194/egusphere-2023-2891>
- Seifert, A., & Beheng, K. D. (2006). A two-moment cloud microphysics parameterization for mixed-phase clouds. Part 1: Model description. *Meteorology and Atmospheric Physics*, 92(1–2), 45–66. <https://doi.org/10.1007/s00703-005-0112-4>
- Sotiropoulou, G., Sullivan, S., Savre, J., Lloyd, G., Lachlan-Cope, T., Ekman, A. M., & Nenes, A. (2020). The impact of secondary ice production on Arctic stratocumulus. *Atmospheric Chemistry and Physics*, 20(3), 1301–1316. <https://doi.org/10.5194/acp-20-1301-2020>
- Stewart, R. E., Thériault, J. M., & Henson, W. (2015). On the characteristics of and processes producing winter precipitation types near 0°C. *Bulletin of the American Meteorology Society*, 96(4), 623–639. <https://doi.org/10.1175/BAMS-D-14-00032.1>
- Sullivan, S. C., Barthlott, C., Crosier, J., Zhukov, I., Nenes, A., & Hoose, C. (2018). The effect of secondary ice production parameterization on the simulation of a cold frontal rainband. *Atmospheric Chemistry and Physics*, 18(22), 16461–16480. <https://doi.org/10.5194/acp-18-16461-2018>
- Sullivan, S. C., Hoose, C., & Nenes, A. (2017). Investigating the contribution of secondary ice production to in-cloud ice crystal numbers. *Journal of Geophysical Research: Atmospheres*, 122(17), 9391–9412. <https://doi.org/10.1002/2017JD026546>
- Takahashi, T., Nagao, Y., & Kushiya, Y. (1995). Possible high ice particle production during graupel–graupel collisions. *Journal of the Atmospheric Sciences*, 52(24), 4523–4527. [https://doi.org/10.1175/1520-0469\(1995\)052<4523:PHIPPD>2.0.CO;2](https://doi.org/10.1175/1520-0469(1995)052<4523:PHIPPD>2.0.CO;2)
- Thériault, J. M., Stewart, R. E., & Henson, W. (2010). On the dependence of winter precipitation types on temperature, precipitation rate, and associated features. *Journal of Applied Meteorology and Climatology*, 49(7), 1429–1442. <https://doi.org/10.1175/2010JAMC2321.1>
- Thompson, G. (2019). High Resolution Numerical Weather model forecasts of icing at the ground and in the air. In *Proceedings of the International Workshop on atmospheric icing of structures* (p. 6). IWAIS. Retrieved from https://iwaais2019.is/images/Papers/042_iwaais_thompson.pdf
- Thompson, G., Rasmussen, R. M., & Manning, K. (2004). Explicit forecasts of winter precipitation using an improved bulk microphysics scheme. Part I: Description and sensitivity analysis. *Monthly Weather Review*, 132(2), 519–542. [https://doi.org/10.1175/1520-0493\(2004\)132<0519:EFOWPU>2.0.CO;2](https://doi.org/10.1175/1520-0493(2004)132<0519:EFOWPU>2.0.CO;2)
- Vardiman, L. (1978). The generation of secondary ice particles in clouds by crystal–crystal collision. *Journal of the Atmospheric Sciences*, 35(11), 2168–2180. [https://doi.org/10.1175/1520-0469\(1978\)035<2168:TGOSIP>2.0.CO;2](https://doi.org/10.1175/1520-0469(1978)035<2168:TGOSIP>2.0.CO;2)
- Xu, M., Thompson, G., Adriaansen, D. R., & Landolt, S. D. (2019). On the value of time-lag-ensemble averaging to improve numerical model predictions of aircraft icing conditions. *Weather and Forecasting*, 34(3), 507–519. <https://doi.org/10.1175/WAF-D-18-0087.1>
- Zhao, X., & Liu, X. (2021). Global importance of secondary ice production. *Geophysical Research Letters*, 48(11), e2021GL092581. <https://doi.org/10.1029/2021GL092581>
- Zhao, X., Liu, X., Phillips, V. T. J., & Patade, S. (2021). Impacts of secondary ice production on Arctic mixed-phase clouds based on ARM observations and CAM6 single-column model simulations. *Atmospheric Chemistry and Physics*, 21(7), 5685–5703. <https://doi.org/10.5194/acp-2020-1276>

References From the Supporting Information

- Gibson, S. R., & Stewart, R. E. (2007). Observations of ice pellets during a winter storm. *Atmospheric Research*, 85(1), 64–76. <https://doi.org/10.1016/j.atmosres.2006.11.004>
- Khairoutdinov, M., & Kogan, Y. (2000). A new cloud physics parameterization in a large-eddy simulation model of marine stratocumulus. *Monthly Weather Review*, 128(1), 229–243. [https://doi.org/10.1175/1520-0493\(2000\)128<0229:ANCPPI>2.0.CO;2](https://doi.org/10.1175/1520-0493(2000)128<0229:ANCPPI>2.0.CO;2)
- Lachapelle, M., Thompson, H. D., Leroux, N. R., & Thériault, J. M. (2023). Measuring ice pellets and refrozen wet snow using a laser-optical disdrometer. *Journal of Applied Meteorology and Climatology*, 63(1), 65–84. in press. <https://doi.org/10.1175/JAMC-D-22-0202.1>
- Lemay, F., & Husson, T. (2017). Emet or forecast verification using the power of a relational database. In *Seventh international verification methods workshop, Berlin, Germany, Deutscher Wetterdienst, P OPS SOFT-7*. Retrieved from https://www.7thverificationworkshop.de/Ressourcen/Annalen_51_komplett.pdf
- Milbrandt, J. A., Morrison, H., Dawson, D. T., II, & Paukert, M. (2021). A triple-moment representation of ice in the Predicted Particle Properties (P3) microphysics scheme. *Journal of the Atmospheric Sciences*, 78(2), 439–458. <https://doi.org/10.1175/JAS-D-20-0084.1>
- Pruppacher, H. R., & Klett, D. (1997). Microphysics of clouds and precipitation. In *Atmospheric and oceanographic sciences library* (Vol. 18, p. 954). Springer.
- WMO (Ed.). (2015). Manual on Codes—International Codes, volume I.1, Annex II to the WMO Technical Regulations: Part A—Alphanumeric Codes. World Meteorological Organization, WMO.